

Fundamentals

This section provides definitions, tools and theory which are relevant for the understanding of the analysis presented in subsequent sections. The first section introduces radiative transfer in the atmosphere and defines parameters required for the Monte Carlo simulations. The measurements and simulations are analysed using power spectra (section 1.2). Previous studies applied this method to radiance measurements and formed the term cloud radiative smoothing, recalled in the last section.

1.1. Radiative transfer and inherent optical properties

The propagation of light through the atmosphere is altered by several atmospheric constituents. Clouds have the most dominant effect on radiative transfer. Their effect depends on many aspects, among them are cloud coverage, macrophysical and microphysical parameters (e.g. cloud thickness and effective radius) as well as thermodynamic characteristics (e.g. phase of cloud particles). Furthermore, aerosols of various type influence radiative transfer in the atmosphere. Like clouds, their spatial distribution and external and internal mixtures are strongly variable. In contrast, the majority of air molecules exhibits a low horizontal variability. However, there are certainly some air molecules which have a significant lateral dependence, e.g. water vapour on a regional to global scale or aerosols during some specific events like sand storms. All constituents exhibit relatively strong vertical variations. This is not only due to pressure and temperature effects but also arises from natural fluctuations.

All these atmospheric constituents interact with solar radiation, either through absorption or scattering. Absorption occurs, if at least one of the energy levels of the particle is suitable for the incident photons energy. The energy is absorbed and remains within the particle. Scattering occurs, if the interaction of particles and photons changes the original direction of the photon. If the size of the particle is small compared to the wavelength of the incident radiation, the particle operates as a Hertz'scher dipole. This form of scattering is named after Lord Rayleigh, and the spectral scattering intensity is proportional to the inverse fourth power of the wavelength, λ^{-4} . If the particle size exceeds the wavelength of the incoming radiation, the spectral dependence of the scattering intensity is negligible and the forward scattering is far more pronounced than for Rayleigh scattering. The results were achieved by *Mie* (1908), and his approach was similar as the one for Rayleigh scattering. But in this case the interference of several dipoles is considered.

All optical relevant atmospheric constituents need to be characterised through their inherent optical properties. The latter means that they depend on the properties of the medium only and not on the ambient light field. The efficiency of absorption and scattering in terms of light attenuation are characterised by the volume absorption and scattering coefficients σ_a and σ_b , respectively. The sum of both coefficients gives the volume extinction coefficient $\sigma_{ext} = \sigma_a + \sigma_b$. All three parameters have units of inverse length. The optical thickness τ is defined as the integral of σ_{ext} over height. The ratio of σ_b to σ_{ext} , the single scattering albedo ω_0 , is a measure for the relative scattering strength of the medium. The single scattering albedo can be interpreted as a probability of photon survival which becomes obvious in section 4.1.

In order to follow a packet of photons, its new propagation direction after each scattering event needs to be predicted. This is done with the help of the volume scattering function

β_{vol} . The integral of β_{vol} over the scattering angle gives the scattering coefficient:

$$\sigma_b = 2\pi \int_0^\pi \beta_{vol}(\psi) \sin\psi d\psi. \quad (1.1)$$

This implies the assumption of symmetric scattering properties with respect to the azimuth of scattering (ψ : scattering angle). Using this relation, the angular dependence of the volume scattering function can be separated from its scattering intensity by normalising β_{vol} on σ_b . This gives the phase function:

$$\tilde{\beta}(\psi) = \frac{\beta_{vol}(\psi)}{\sigma_b}. \quad (1.2)$$

From equations 1.1 and 1.2 follows the normalisation condition of the phase function:

$$2\pi \int_0^\pi \tilde{\beta}(\psi) \sin\psi d\psi = 1. \quad (1.3)$$

If warm clouds are considered, and not ice or various aerosol particles, $\tilde{\beta}$ depends on the cloud droplet number distribution $n(r)$ and the wavelength. Using Mie theory (*Mie*, 1908) $\tilde{\beta}$ can be determined at a certain wavelength and for each radius of a given distribution. The final phase function is calculated by averaging each $\tilde{\beta}$ weighted by its frequency of occurrence. The effective radius r_{eff}

$$r_{eff} = \frac{\int r^3 n(r) dr}{\int r^2 n(r) dr} \quad (1.4)$$

is frequently used to characterise a cloud droplet number distribution.

It was mentioned previously in this section that scattering may emphasise the forward scattering direction. This reaction can be characterised by the asymmetry factor which is the average over all scattering directions of the cosine of ψ . It is close to one, if the forward scattering is pronounced, and zero, if the phase function is symmetric about $\psi=90^\circ$. Multiple scattering significantly increases the photon path which in turn increases the amount of absorbed photons. Radiative transfer, especially absorption aspects, are complicated by multiple scattering between cloud parcels, between cloud and surface, and between different cloud layers.

Another process is inelastic scattering by air molecules. After the absorption of photons and the excitation of virtual energy levels, the molecules return to a state of higher (lower) energy than they had before excitation. The re-emitted photon is characterised by a smaller (higher) wavelength than the absorbed photon. This process can be effective in the UV and is neglected in this work.

1.2. Power spectrum analysis

A frequently used method to characterise geophysical data sets is the (spatial) power spectrum analysis. Among these data sets are spatial high-resolution observations of nadir radiances reflected by cloud decks. Recent studies focused on satellite measurements and radiative transfer simulations of the nadir radiance (e.g. *Boers et al.*, 1988; *Cahalan and Snider*, 1989; *Fischer et al.*, 1991; *Oreopoulos et al.*, 2000), while this work concentrates on airborne remote sensing observations and radiative transfer simulations.

Prior to the power spectrum analysis the radiance data is preprocessed to minimise artificial effects that may arise if the analysis is applied to the original data set. One of these impacts can arise from a linear trend in the data set. The linear trend can result in a significant increase of the power spectrum at large wave numbers. The mean linear trend is subtracted to deal with the problem. A second reason for artefacts can be that the start and end value of the data set are not similar. In this case windowing is applied to the data set which means that the set is shortened appropriately. Figure 1.1 shows an example of windowing and is based on nadir radiances at 620 nm measured with an airborne imager on 06 September 2001 (see sections 2.1.1 and 2.2). Approximately 100 values are omitted in this case.

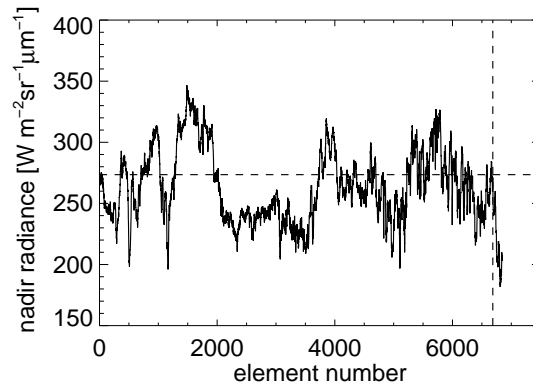


FIGURE 1.1. Nadir radiance at 620 nm versus element number. The dashed vertical line indicates the element number where, starting from largest element numbers, the first value is within $\pm 2.5\%$ of the value with element number 0 (marked with a horizontal dashed line). The data was recorded with *casi* on 06 September 2001, and the figure is redrawn from *Schröder et al.* (2004).

The power spectrum, $E(k)$, is calculated by the absolute square of the Fourier transformed radiances. The imaginary part of the transformed data is not omitted. If the following behaviour is given:

$$E(k) \sim k^{-\beta} \quad (1.5)$$

the radiance is considered to be scale-invariant, where k is the wave number, $r = 1/k$ the corresponding scale and β the slope. The discrete nature of the radiance measurements give reason to some special features if the Fourier transformation is applied: If the radiance data set consists of N data points, then the Fourier transformation provides useful data only at wave numbers within the interval $[\frac{1}{N\Delta r}, \frac{1}{2\Delta r}]$, with Δr being the smallest scale and $k_{\text{Nyquist}} = \frac{1}{2\Delta r}$ being the Nyquist wave number. Due to the symmetry of the Fourier transformation, all wave numbers larger than k_{Nyquist} are redundant and are not shown in the following. Another aspect is the aliasing effect. If the sampling rate is not high enough, i.e. the signal contains frequencies larger than half of the sampling rate, components of the signal at high frequencies are mirrored at f_{Nyquist} (f_{Nyquist} : Nyquist frequency) and contribute to components at lower frequencies. Here it is assumed that the sampling rate is high enough to avoid aliasing. Finally, the finiteness of the data set is interpreted as the convolution of the data set and a rectangular function by the discrete Fourier transformation. The effect of the discrete jump at the start and end of the data set on the transformation can be reduced by applying special filters. The most common ones are the Hanning or Hamming filters which cause the modified data set to be continuous at its end. The application of the filters is named apodisation and is not carried out here because it is not possible to maintain similar qualities of the apodisation for different data sets.

The binning procedure introduced by *Davis et al.* (1996), where more details on power spectrum analysis are given, is adapted. Here, the binning is conducted in factors of two in k (octave binning): 2^m with $m \in [0, 1, \dots, \log_2 N_{\text{tot}} - 2]$. N_{tot} is the total number of energy values and $\log_2 N_{\text{tot}}$ the largest integer power of two less than N_{tot} . A sequence of wave number bins with increasing wave number is created, and the corresponding energy is averaged over the appropriate wave numbers. The binning reduces the noise level and ensures that all scales contribute equally, i.e. it avoids that the accumulation of energy values at small scales of the interpolation range dominates the least square fit (see next paragraph), if the non-binned, original power values are used.

If the power spectrum analysis is applied to nadir radiance measurements, typically two ranges of scale invariance can be observed. One is found at large scales between ~ 0.5 and ~ 20 km and one at small scales between ~ 0.025 and ~ 0.3 km. Each of the scale regions is interpolated by a least square fit. A small region around the scale break is excluded from the interpolations. If bins at large scales deviate significantly from the overall large scale invariance, they are also omitted from interpolation. The scale break is determined by the interception of the linear approximations at large and small scales. Figure 5.11 shows two examples of the application of the power spectrum analysis. The dots present the original power spectrum, the squares the binned spectrum and the solid line the outcome of the linear regression.

The scale breaks as well as the small and large scale slopes are affected by linear interpolation errors. The impact of these uncertainties on the parameter determination is estimated by subsetting each bin which was defined during the binning procedure and are used for linear regression. Instead of using the complete original set of energies, half of the total amount of values in each bin is randomly chosen. This random process produces a set of slopes and scale breaks. The standard deviation of these values is used as an uncertainty measure for the scale break and the large and small scale slope. In addition, these uncertainties are averaged over regions of constant reflectivity and therefore change by a factor of $N^{-1/2}$, with N being the number of channels used for averaging.

The slope β is a measure for the degree of stationarity. A signal is considered stationary if its ensemble average does not depend on the location. If ergodicity is assumed, the spatial and the ensemble average are equivalent, and the small scale average of the signal is representative for the whole data set. If β is smaller than one than the signal is stationary, if it lies between one and three, the signal has stationary increments. Usually, the large scale slope related to observed nadir radiances follows the 5/3 power law found in isotropic turbulence while the small scale slope is generally slightly smaller than three.

An independent verification of the power spectrum analysis is recommended. An opportunity for the verification offers the structure function analysis which is introduced by *Marshak et al. (1997)* in great detail. If the data set is scale invariant and has stationary increments, then the scale dependent differences are not a function of the location x . It follows:

$$\langle |\Delta L(r; x)|^q \rangle = \langle |\Delta L(r)|^q \rangle = \langle |L(x+r) - L(x)|^q \rangle \sim r^{\zeta(q)} \quad (1.6)$$

with $L(r; x)$ denoting the data set and q being the q -th moment. The outer brackets indicate that ensemble averages should be conducted. Usually, local averages are determined which implicitly assumes ergodicity. Under the previously made assumptions the Wiener-Khinchine theorem can be interpreted as follows (*Davis et al., 1994*):

$$1 < \beta = \zeta(q=2) + 1 < 3. \quad (1.7)$$

This equation is used to verify the power spectrum analysis in scale-invariant regions if stationary increments are given.

The power spectrum analysis may not be the appropriate tool to characterise observational data in a unique way. If, e.g., white noise and δ -functions are subject of the analysis, both result in scale invariant behaviour with $\beta = 0$. The ambivalence is not found in structure function analysis. However, the investigation of cloud radiative smoothing is carried out with power spectrum analysis (section 5).

1.3. Plane-parallel bias and horizontal photon transport

A few general aspects and consequences of 1d, 2d, and 3d radiative transfer are discussed here. Three main types of radiative transfer models and corresponding assumptions are widely applied: the plane-parallel model, the independent pixel approximation and 3d Monte Carlo simulations. The plane-parallel model allows vertical layering but is restricted to horizontally homogeneous layers. If the dependence of nadir reflectances on optical thickness is considered this may lead to significant uncertainties. In general, the following

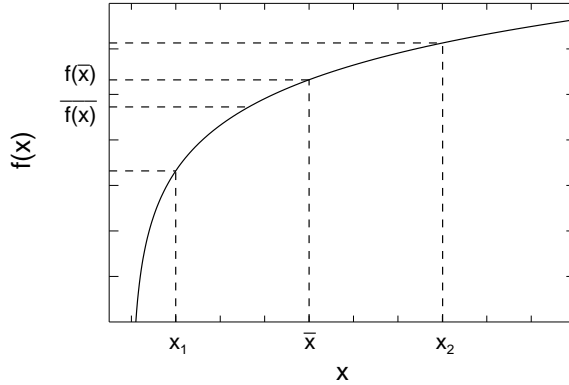


FIGURE 1.2. Sketch to illustrate the plane-parallel bias. The function $f(x)$ reflects a similar course than the dependence of the reflectance on optical thickness. The non-linear behaviour of the relation results in different reflectances if averaging in x or $f(x)$ is considered.

relation is valid: $R(\bar{\tau}) \geq \overline{R(\tau)}$, and the discrepancy can reach 17% (Cahalan *et al.*, 1994). This phenomenon is explained in Figure 1.2. The figure shows a sketch of a function which dependence on x is generally comparable to the optical thickness-reflectance relation. The curvature of the graph is the reason that $f(\bar{x})$ is always equal or larger than $\overline{f(x)}$. Identity is given for an infinitesimally small range of x . In reality not only the functional context but also the lateral distribution of the pair of variables effects the bias.

The plane-parallel bias can be avoided, if the independent pixel approximation (IPA) is utilised. In the frame of this method the horizontal variability of e.g. the optical thickness is approximated by an appropriate number of grids. On each grid the plane-parallel model is applied. The IPA does not allow photons to travel horizontally between different boxes. This can lead to significant deviations from precise 3d radiative transfer simulations: Cahalan and Snider (1989) first observed a scale break in power spectra derived from Landsat data and were able to explain this by horizontal photon transport. The spectral behaviour of horizontal photon transport on reflected and transmitted solar radiation has been investigated intensively by Marshak *et al.* (1995a) and Davis *et al.* (1996, 1997a). The semi-heuristic relation for the transmission case, which states that the scale break is proportional to the geometrical thickness of the cloud, was verified by von Savigny *et al.* (1999) who used zenith radiance observations for this purpose.

Assuming plane-parallel layering and conservative scattering Davis *et al.* (1997a) carried out a simple radiative transfer experiment to quantify horizontal photon transport. By injecting photons in the centre of a model cloud they determined the photons horizontal displacement vector, i.e. the horizontal distance between the point of injection and escape. With regard to the reflection case, they found an expression which relates the radiative smoothing scale η to cloud properties:

$$\eta \sim H / \sqrt{(1-g)\langle\tau\rangle}. \quad (1.8)$$

H is the cloud thickness, g the asymmetry factor and $\langle\tau\rangle$ the mean optical thickness. In a conservative medium horizontal photon transport causes high frequencies, which appear in the optically relevant cloud properties (e.g. the optical thickness), to be smoothed out in the observed nadir radiance. This effect is illustrated in Figure 1.3. In this way, the high frequencies of the optical thickness distribution do not contribute to the power spectrum at high frequencies. It explains the occurrence of the scale break and the increased small scale

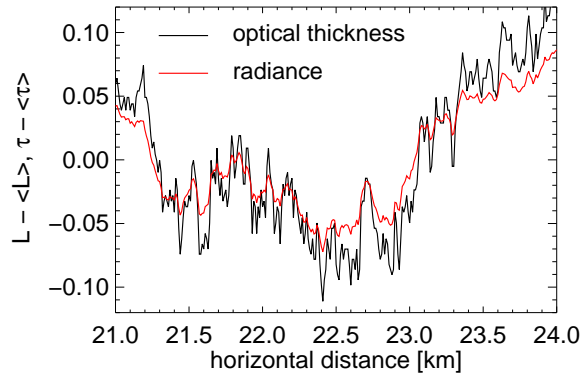


FIGURE 1.3. Mean free normalised reflectance and optical thickness versus distance. The figure shows fragments of the cloud field and simulated reflectance from section 5.2.

slope and has been denoted as cloud radiative smoothing. Since cloud radiative smoothing is due to horizontal photon transport, the scale break cannot be reproduced with IPA simulations. 200-500 m is a typical variability of observed scale breaks for stratocumulus clouds.